# Navier-Stokes Analysis of Pitching Delta Wings in a Wind Tunnel

**Yung-Gyo Lee***
Airship Research Group
Korea Aerospace Research Institute, Daejon, Korea, 305-600

## Abstract

A numerical method for the assessment and correction of tunnel wall interference effects on forced-oscillation testing is presented. The method is based on the wall pressure signature method using computed wall pressure distributions. The wall pressure field is computed using unsteady three-dimensional full Navier-Stokes solver for a 70-degree pitching delta wing in a wind tunnel. Approximately-factorized alternate direction implicit (AF-ADI) scheme is advanced in time by solving block tri-diagonal matrices. The algebraic Baldwin-Lomax turbulence model is included to simulate the turbulent flow effect. Also, dual time sub-iteration with local time stepping is implemented to improve the convergence. The computed wall pressure field is then imposed as boundary conditions for Euler re-simulation to obtain the interference flow field. The static computation shows good agreement with experiments. The dynamic computation demonstrates reasonable physical phenomena with a good convergence history. The effects of the tunnel wall in upwash and blockage are analyzed using the computed interference flow field for several reduced frequencies and amplitudes. The corrected results by pressure signature method agree well with the results of free air conditions.

**Key Word** : Unsteady, Full Navier-Stokes, Delta Wing, Wall Interference

## Introduction

Delta wing configurations are adopted for several modern fighters to obtain high maneuvering capabilities at high angles of attack. At low angles of attack, the viscous shear layers are confined to separation bubbles near the surface with small effects on the aerodynamic characteristics. Thus, linear lift variation with the angle of attack is typical. The flow conditions at high angles of attack involve vortex flow, generated at the sharp leading edges due to the roll up of free shear layer, vortex bursting, interference from the low-energy wakes. These phenomena lead to nonlinear lift variation with the angle of attack. At even higher angles of attack, unsteady turbulent wake and post stall characteristics take place. This process is called the static stall.

However, when dynamic motion is involved, for example, for a pitching delta wing at a certain reduced frequency, the unsteady effects will fundamentally change the aerodynamic characteristics. The hysteresis loop, caused by the lag in flow separation and reattachment and/or vortex bursting, is a phenomenon of unsteady flow field with a pitching delta wing. The extent of these changes depends on the parameters such as the pitch-rate, pitching amplitude, motion history, free stream Mach number.

* Senior Researcher
E-mail : lyg@kari.re.kr, TEL : 042-860-2353, FAX : 042-860-2009

The hysteresis loop may cause stability and control problems in abnormal flight conditions including gust or turbulence encounter. Such unsteady aerodynamic conditions are typically not considered in the current design process.

Numerous subsonic experimental studies were made to investigate the flow structures over steady/unsteady delta wings. Wentz[1] conducted a comprehensive static experimental research on delta wings with various apex angles. He correlated static force measurements to flow visualization to show the relationship between leading edge vortex formation, bursting and the forces and moments on the wing. More recently research has focused on oscillating delta wings. Flow visualization has shown hysteresis loops in the measured vortex burst locations. Wolffelt[2], Soltani et al.[3], and Torlund[4] have all reported force and moment data on oscillating delta wings.

At the same time, many numerical efforts were made to simulate the flow field around delta wings. An early calculation of the static flow around a delta wing by thin-layer Navier-Stokes was presented by Fujii and Kutler in 1984. Numerical static solutions of delta wings by the thin-layer approximation of the Navier-Stokes equations were also used in the calculations of Fujii and Schiff[5], Hartwich et al.[6] and Ekaterinaris et al.[7]. For roll-oscillating delta wings, thin-layer Navier-Stokes solvers were used by Kandil and Chuang[8] and Chaderjian et al.[9]. But, to the author's knowledge, no numerical solution has been reported on pitching delta wings by using full Navier-Stokes solvers. The latter can better resolve the flow variables in the separated flow region.

For a validation of the numerical predictions, accurate experimental data are necessary. However, the experimental data with which comparisons are made are taken inside wind tunnels where several influencing factors need to be evaluated and treated correctly. Among the factors the wall interference effect is important, particularly in the case of solid tunnel walls. Some significant effects of solid walls are the increase of the overall angle of attack by reduction of downwash, a change of the streamline curvature, an alteration of local angles of attack and dynamic pressure increase due to the blockage. The correction methods of wall interference are presented in detail in Ref. [10] from the classical methods by a linear theory to the pressure signature method.

Due to the rapid advance of modern computer technology, computational fluid dynamics method can now be employed for wall interference correction. Thomas and Lan[11] and Hsing and Lan[12] used thin-layer Navier-Stokes equations to simulate the static test environment in the wind tunnel. Calculated static pressure distributions on the tunnel walls were used to compute the wake blockage and upwash effects on the model.

Wind tunnel wall interference in unsteady tests has not been as thoroughly investigated as in steady tests. Unsteady wind tunnel effects consist of two parts[10];

- undisturbed base flow and steady perturbations
- purely unsteady sources of interference

The purely unsteady sources of interference are :

- unsteady effects of wall constraint
- reflection of model generated acoustic disturbances by the wall
- acoustic wind tunnel resonance
- distortion and termination of the oscillatory wake of the model
- inherent tunnel flow fluctuations
- interference of large model oscillation devices and supports

For the complex unsteady flow field, most of the traditional interference correction methods including the measured wall pressure signature method have not matured yet.

In the current research, three dimensional unsteady full Navier-Stokes equations are employed to investigate the unsteady wall interference effects for pitching delta wings in a wind tunnel. For the wall pressure signature method, the computed wall static pressure distributions and their variations with time are saved in the form of Fourier series to reduce

the data storage. These data are then used to compute the interference flow field during the Euler re-simulation process.

## Numerical Schemes

Three dimensional unsteady Reynolds-averaged full Navier-Stokes solver in conservation form are used to compute the flowfield around pitching delta wings. The steady state thin-layer Navier Stokes code, KUNS3D is modified to accommodate unsteady computations with moving grid systems. The KUNS3D of the University of Kansas is a modified version of ARC3D[13] for the computation of model in tunnel and interference flow field.

Written in generalized curvilinear coordinates, the code solves the following unsteady full Navier-Stokes equations.

$$\hat{Q}_\tau + \hat{E}_\xi + \hat{F}_\eta + \hat{G}_\zeta = \hat{E}_{v_\xi} + \hat{F}_{v_\eta} + \hat{G}_{v_\zeta} \tag{1}$$

where

$$\hat{Q} = J^{-1}\begin{bmatrix}\rho\\ \rho u\\ \rho v\\ \rho w\\ e\end{bmatrix} \quad \hat{E} = J^{-1}\begin{bmatrix}\rho U\\ \rho uU+\xi_x p\\ \rho vU+\xi_y p\\ \rho wU+\xi_z p\\ U(e+p)-\xi_t p\end{bmatrix} \quad \hat{F} = J^{-1}\begin{bmatrix}\rho V\\ \rho uV+\eta_x p\\ \rho vV+\eta_y p\\ \rho wV+\eta_z p\\ V(e+p)-\eta_t p\end{bmatrix} \quad \hat{G} = J^{-1}\begin{bmatrix}\rho W\\ \rho uW+\zeta_x p\\ \rho vW+\zeta_y p\\ \rho wW+\zeta_z p\\ W(e+p)-\zeta_t p\end{bmatrix} \tag{2}$$

Q is the solution vector and E, F and G are the inviscid flux vectors. Detailed expressions of the viscous flux vectors $E_v$, $F_v$ and $G_v$ can be found in Ref[14].

With the implicit approximate factorization algorithm, the above three dimensional equation (1) is simplified to the following form. The central-difference scheme for all space derivatives is used without degrading the time accuracy of any second order scheme[13].

$$\begin{aligned}&\left[I + h\delta_\xi \hat{A}^n - h\,\mathrm{Re}^{-1}\delta_\xi J^{-1}\hat{L}^n\right]\left[I + h\delta_\eta \hat{B}^n - h\,\mathrm{Re}^{-1}\delta_\eta J^{-1}\hat{M}^n\right]\left[I + h\delta_\zeta \hat{C}^n - h\,\mathrm{Re}^{-1}\delta_\zeta J^{-1}\hat{N}^n\right]\Delta\hat{Q}^n\\ &= -h\left(\delta_\xi \hat{E}^n + \delta_\eta \hat{F}^n + \delta_\zeta \hat{G}^n - \mathrm{Re}^{-1}(\delta_\zeta \hat{E}_v{}^n + \delta_\eta \hat{F}_v{}^n + \delta_\zeta \hat{G}_v{}^n)\right)\end{aligned} \tag{3}$$

Implicit viscous terms in equation (3) are neglected to increase the efficiency of the algorithm. In practice, it produces identical stability and less computational work. The implicit part is written as the block tridiagonal matrices in the computational algorithm, which is solved by block LUD (lower-upper decomposition) using locally one dimensional matrix inversions. In the ARC3D, this equation is simplified to the scalar penta-diagonal form for steady state, first order time accurate computations.

For unsteady flow, second order time accurate methods are used. The flow field is initialized from the steady state solution and integrated forward in time. By ignoring all viscous flux Jacobians , the second order AF-ADI scheme can be written as in equation (4).

For the viscous-separated and/or vortical flow fields, the full Navier-stokes equations, as opposed to the thin-layer approximation, are used for improved resolution of all flow field characteristics. This means all the viscous terms associated with the $\zeta$ and $\xi$ derivatives are retained in the equations as well as the $\eta$ derivatives.

$$\begin{aligned}&\left[I + \frac{2}{3}h\delta_\xi \hat{A}^n\right]\left[I + \frac{2}{3}h\delta_\eta \hat{B}^n\right]\left[I + \frac{2}{3}h\delta_\zeta \hat{C}^n\right]\Delta\hat{Q}^n\\ &= \frac{1}{3}\Delta\hat{Q}^{n-1} - \frac{2}{3}h\left(\delta_\xi \hat{E}^n + \delta_\eta \hat{F}^n + \delta_\zeta \hat{G}^n - \mathrm{Re}^{-1}(\delta_\zeta \hat{E}_v{}^n + \delta_\eta \hat{F}_v{}^n + \delta_\zeta \hat{G}_v{}^n)\right)\end{aligned} \tag{4}$$

To assure the numerical stability, Jameson's artificial dissipation terms are added to the complete algorithm without affecting the accuracy of any physical viscous effects. Explicit and implicit artificial dissipation terms are added to the right and left hand side of equation (4) respectively, to achieve nonlinear stability.

Spatially variable time step is used to accelerate convergence for the steady state and pseudo time sub-iteration computations. The time step $\Delta t$ is re-scaled using the multiplication factor based on eigenvalues. Also, the algebraic turbulence model of Baldwin and Lomax is implemented. To represent turbulence effectively in this model, the minimum y+ should be below 5.0.

The grid systems of a delta wing in a tunnel and free air is based on O-H mapping as can be seen in Fig. 1. To simulate a delta wing in pitching motion, the initial grid system for a fixed angle of attack is generated and used to compute the steady state solution. And then, during dynamic computation, the surface grids are moved according to the prescribed angular velocity. The grid speed is allowed to decay along the normal distance to zero at the outer boundaries. The grid speeds are also explicitly obtained in the process since the algebraic equations involve the grid speeds.

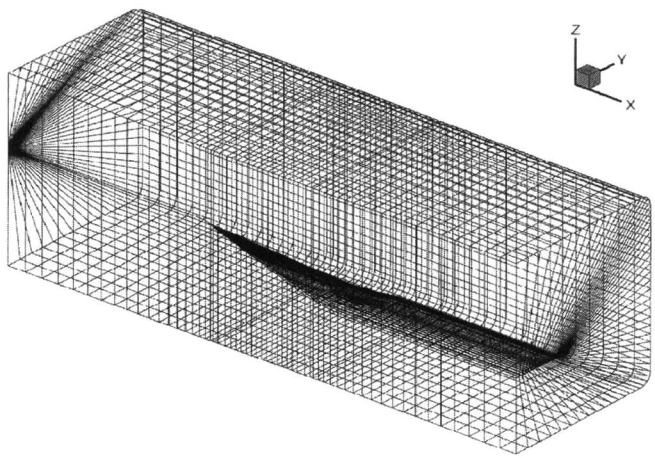


**Fig. 1. Two block grid system for a 70° delta wing in a tunnel**

At the body surface, the no-slip condition must be satisfied in a viscous flow field; the contravariant velocities, U, V and W are set to zero on the solid surface. At the free stream lateral boundaries, a non-reflective characteristic-like boundary condition is used. The locally one-dimensional Riemann invariant boundary condition is used at the inlet surface. For outlet boundary conditions, flow variables are extrapolated from the interior except pressure, which is fixed to be the free stream value. For the matched simple interface of two blocks, it is straightforward to apply the boundary conditions when overlapped zonal grids are employed, because the boundary conditions for a block are directly injected from the interior of the other block[9]. In the present calculation, the inner and outer blocks are overlapped each other by one layer. For the interference flow field computation, flow-through boundary condition on the model surface is used, while the far field boundary conditions are fixed to the free stream properties except pressure. Computed wall pressure distributions are imposed on the far field boundary. Thomas and Lombard pointed out the need to maintain global conservation on moving grids. Geometric Conservation Law (GCL) is essential for moving grids. In current research, the Jacobian of transformation is computed every time step to satisfy the continuity equation for motionless flow field with grid movements.

**Dual Time sub-iteration**

The dual time sub-iteration presented here is based on the CFL3D method of NASA Langley Research Center. Adding pseudo time term to equation (4), we get

$$\frac{1}{J}\frac{\partial Q}{\partial \tau}+\frac{(1+\phi)(Q^{n+1}-Q^{n})-\phi(Q^{n}-Q^{n-1})}{J\Delta t}=R(Q^{n+1}) \tag{5}$$

Equation (5) is then discretized and iterated in m, where m is the sub-iteration number,

$$\left[\left(\frac{1+\phi'}{J\Delta\tau}+\frac{1+\phi}{J\Delta t}\right)I+\delta_{\xi}A^{m}+\delta_{\eta}B^{m}+\delta_{\zeta}C^{m}\right]\Delta Q^{m}=\frac{\phi'\Delta Q^{m-1}}{J\Delta\tau}+\frac{\phi\Delta Q^{n-1}}{J\Delta t}-\frac{(1+\phi)(Q^{m}-Q^{n})}{J\Delta t}+R(Q^{m}) \tag{6}$$

$$Q^{m+1} = Q^{m} + \Delta Q^{m} \tag{7}$$

As m goes to infinity in equation (6), the pseudo time term vanishes if sub-iterations converge and eventually, $Q^{m+1}$ becomes $Q^{n+1}$. This is the concept of sub-iteration and of adding ($Q / J\Delta\tau$) term on the left hand side. In practice, just a few sub-iterations are enough for a converged solution. By using the ADI (Alternate Direction Implicit) scheme with first order pseudo time accuracy, the equations are solved as a series of sweep in each direction. It is difficult to find an optimal value of $\Delta\tau$ because convergence is improved continuously and slowly as $\Delta\tau$ increases. But, it is known that a very large $\Delta\tau$ makes the scheme unstable. The quantity $\Delta\tau$ is usually $10^4$ - $10^5$ times the physical time step, $\Delta t$. $\Delta\tau$ of 100 is used in the current research.

Since the computed wall pressure at each grid point varies with time, and the time step is small, it would require a large storage space to store these data for processing. One solution to this problem is to use a Fourier series representation. $C_p(t)$ is defined in the interval C < t < C+Period and approximated by Fourier series. Numerical integration can be done easily using the trapezoidal rule for these Fourier coefficients. Instead of the huge wall pressure data file, Fourier coefficients are stored and used in Euler re-simulation process as the wall boundary conditions.

**Wall Pressure Signature Method**

The correction technique used in the current research is based on the calculated tunnel wall pressure data. The pressure signature obtained from the Navier-Stokes computation is used as the boundary condition for an Euler re-simulation of the tunnel domain without the model. This produces an interference flow field which contains and ($q_c/q$) information that can be used to correct forces and moments. For this re-simulation process, the pressure signature is the only variable specified on the outer domain boundaries. Therefore, the tunnel wall boundaries become force-free transpiration boundaries.

With the upwash and dynamic pressure information obtained from the wall pressure signature method, the corrected angle of attack can be determined using the velocity changes due to the wall.

$$\alpha_c=\alpha+\Delta\alpha \tag{8}$$

where, $\Delta\alpha = \tan^{-1}(\Delta w/(U+\Delta u))$

The correction to dynamic pressure by the blockage effect is determined from

$$\frac{q_c}{q_\infty}=\frac{\left[(U_\infty+\Delta u)^2+\Delta w^2\right]}{U^2{}_\infty} \tag{9}$$

Both the upwash and blockage corrections are determined by averaging those values on the whole wing surface location in the interference flow field.

The force and moment coefficients corrected for the blockage effect are

$$C_L = L / q_c S , \quad C_D = D / q_c S \quad \text{and} \quad C_m = M / q_c S \tag{10}$$

These coefficients are the values plotted at $\alpha_c$, instead of $\alpha$, to complete the upwash correction.

## Results and Discussion

### Test Models

The reference test model for the computation is described in Ref [15]. A 70-degree delta wing, constructed of a flat plate (0.024 thickness to chord ratio) with sharp beveled leading and trailing edges, was used. The tunnel test section of the Ohio State University is 5 feet wide, 3 feet high, and 8 feet long. With the root chord length of the model being 20.61 inch, the test section size results in 2.91 x 1.75 root chord length. A Mach number of 0.14 and Reynolds number of 1 x $10^6$ (based on the root chord length) are used. For the dynamic computations, 4 cases are computed in free air and in the wind tunnel. Reduced frequencies are based on the half mean aerodynamic chord. The four cases of computation are ;

- Code Validation : k=0.0376, $\alpha_{mean} = 27.0^\circ$ , $\alpha_{amp} = 17.0^\circ$
- Case 1 ; Reference, k=0.167, $\alpha_{mean} = 20.0^\circ$ , $\alpha_{amp} = 5.0^\circ$
- Case 2 ; Low frequency, k=0.067, $\alpha_{mean} = 20.0^\circ$ , $\alpha_{amp} = 5.0^\circ$
- Case 3 ; Large Amplitude, k=0.167, $\alpha_{mean} = 20.0^\circ$ , $\alpha_{amp} = 10.0^\circ$

Pitching moments are computed and transferred along the wing stations according to the experimental conditions.

The static experimental data are taken from Ref. [1]. The test model was 18 inch long with chamfered edges and the tunnel size was 4 feet wide and 3 feet high. The test Reynolds number was 1 x $10^6$ (based on the wing root chord). Pitching moments were taken at 50% wing root chord station.

In addition, the experimental results of Ref. [16] are used for comparison of static and dynamic computations. The model is 18 inch long with beveled edges and the experiments were done in the NASA Langley's 12-foot Low speed wind tunnel. The mean angle of attack and amplitude are 27.5 degrees with the Reynolds number up to 0.4 million per foot (based on the mean aerodynamic chord). Center of rotation and pitching moment were taken at 40 % mean aerodynamic chord.

For the code validation, computed results are referenced to the same center of pitching moment as the experimental results. For the Cases 1 through 3, 25% root chord station of the center of pitching moment is used according to the Ref. [15].

### Code Validation

In Figs. 2 - 4, the computed static data are compared to the wind tunnel measurements of Ref. [1]. The results show excellent agreement on $C_L$ and $C_D$ with Wentz's[3] experiments, even beyond the angle of attack where the vortex breakdown occurs. According to Ref. [1], vortex breakdown occurs at the trailing edge at $\alpha = 30^\circ$ in agreement with the present computation. $C_M$ shows larger discrepancy because the computed leading edge vortices are located closer to the trailing edge than the data shown. This situation will make the correction of the static pitching moment curve much more difficult because of the fundamental change in the local loading. The comparison is also made with results of Ref. [16]. In Fig. 5, the experimental normal force coefficients are significantly lower than the computed ones. The reason for the inconsistency in these two sets of data is not known. However, the computed

results always show that for a model in the tunnel, $C_L$ and $C_D$ are higher than in free-air conditions. In the experiments of Ref. [16], vortex breakdown at the trailing edge occurs at $\alpha$ = 22.5° , causing significant differences in flow characteristics as well as the magnitude of aerodynamic coefficients from Ref. [1] and the present computations.

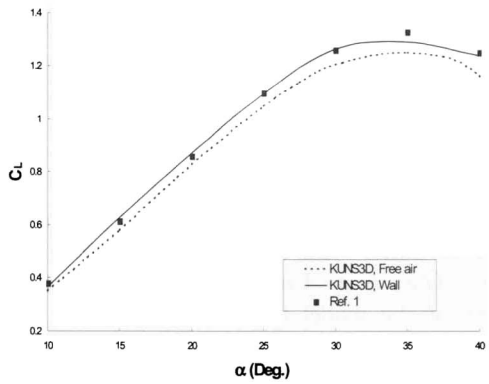


Fig. 2. Comparison of static computations

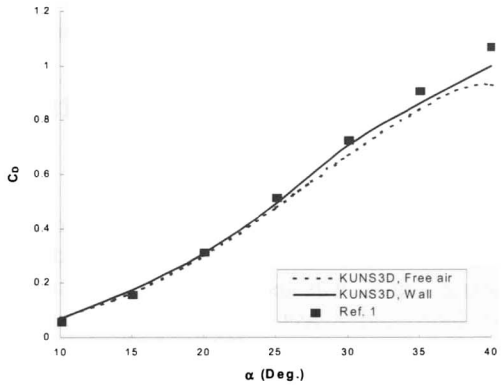


Fig. 3. Comparison of static computations

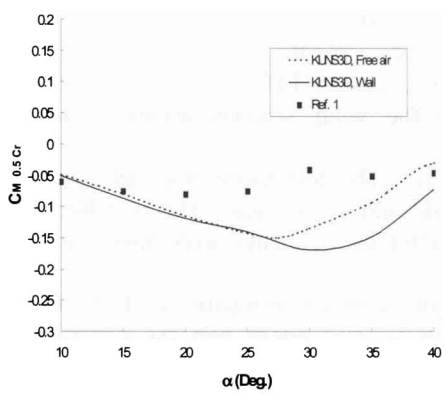


Fig. 4. Comparison of static computations

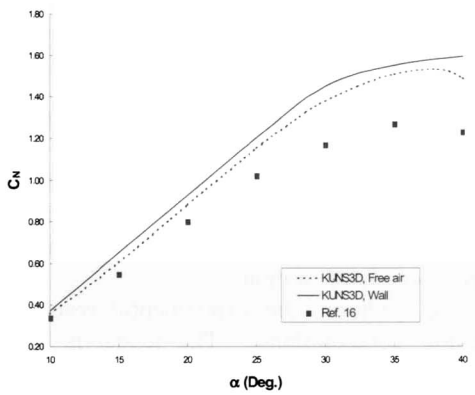


Fig. 5. Comparison of static computations

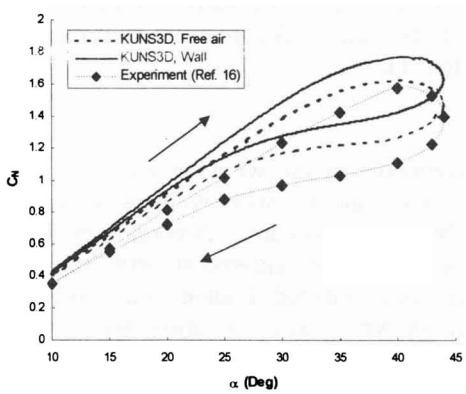


Fig. 6. Comparison of dynamic computations

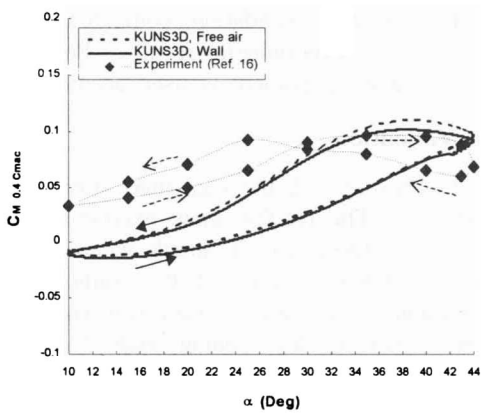


Fig. 7. Comparison of dynamic computations

For dynamic computation, k = 0.0376, $\alpha_{mean}$ = 27° and $\alpha_{amp}$ = 17° are used to check the algorithm and to survey the flow field. One and half cycles appear to be sufficient to get a converged solution. With a non-dimensionalized time step of 0.009, it corresponds to 20000 time steps and about 170 hours of CPU time is required on the SGI Origin 2400™'s 400MHz single processor. At each time step, 5 sub-iterations are performed, but 10 sub-iterations are required for angles of attack higher than 30.0 degrees. The dynamic test data of Ref. [16] are presented in Figs. 6-7 together with the present computed results. Although hysteresis loops caused by the dynamic motion can be predicted for the normal force and pitching moment curves, the discrepancy in $C_N$ basically shows the same trend as in the static data. However, the experimental pitching moment curve shows a counter-clockwise loop below about 30, implying positive pitch damping, but a clockwise loop for $\alpha > 30$, implying negative pitch damping. In the experiments of Ref. [16], it was reported that $\alpha$ = 30 was roughly the angle of attack at which the vortex bursting point was at the trailing edge during pitch up, while it was at the trailing edge at $\alpha$ = 18 during down stroke. As will be seen later, however, vortex breakdown is located at the trailing edge at $\alpha$ = 35 to 43 during pitch up, and $\alpha$ = 35 to 25 during pitch down in the current predictions. The angle of attack, at which vortex breakdown occurs on the wing, causes significant changes in longitudinal stability. On the other hand, the predicted pitching moment curve shows positive damping only, as in the experimental data for $\alpha < 30$. This is because the present computation does not show the dynamic vortex breakdown effect similar to the experimental data of Ref. [16] within the range being examined. Fig. 8 indicates good convergence history in both static and dynamic computations. The residual decreases during static computation and stays at the same level during dynamic computation. After complete convergence, the residual in dynamic computation is repeated along the cycle of pitching motion.

Although not plotted in this paper, the pressure on the rear portion of the wing is lower during up stroke than during down stroke over a large area, resulting in more pitch down moment. However, as $\alpha$ is increased to 43, the area with lower pressure is shifted forward presumably because the vortex bursting point has not yet reached the apex and the vortex is strong and close to the planform in that area. This results in increase of pitch up moment. This phenomenon is continued down to $\alpha$ = 35° , producing more positive pitching moment. Restoration of unburst vortex core does happen when the angle of attack reaches about 25° resulting in the hysteresis characteristics of aerodynamic coefficients.

Therefore, it may be concluded that the predicted positive pitch damping is caused by the delayed vortex break down compared to the earlier bursting in the experimental results of Ref. [16] causing negative pitch damping.

In Figs. 9-10, computed wall pressure distributions are presented. Lower pressure develops on the top of the tunnel, while higher pressure grows on the bottom surface. During down stroke the wall pressure tends to be more positive everywhere than that during up stroke at the same angles of attack.

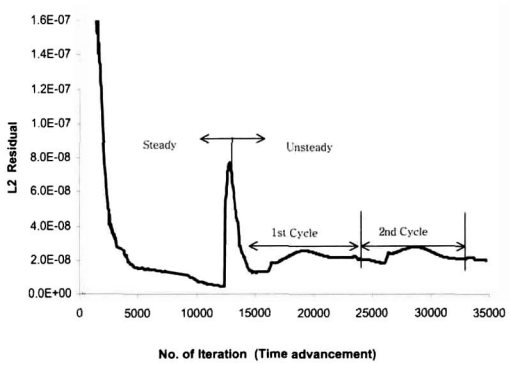


Fig. 8. Convergence history

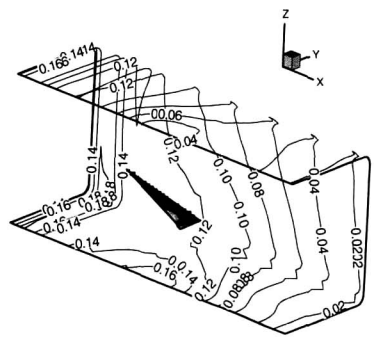


Fig. 9. Wall surface pressure distribution, $\alpha$ = 25 °, Up

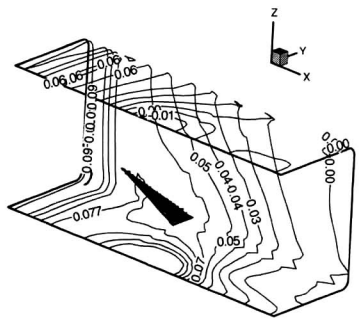


Fig. 10. Wall surface pressure distribution, $\alpha$ = 25 °, Down

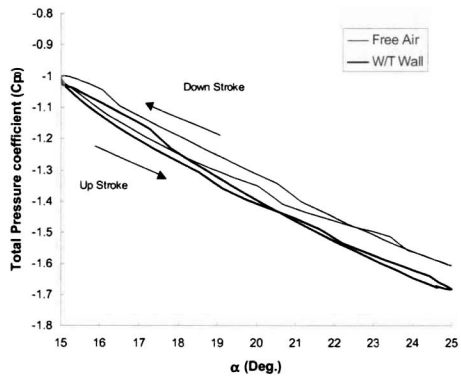


Fig. 11. Vortex Core Strength (Case 1)

## Evaluation of Wall Effects on Aerodynamics

As pointed out in Ref. [16], as the reduced frequency and amplitude of oscillation are increased, the hysteresis is enhanced. Also, the model in the tunnel develops higher lift and drag coefficients, and greater pitch down moment. For example, during up stroke at $\alpha$ = 20 in the large amplitude oscillation, $C_L$=0.88 in free air and $C_L$=0.93 in the 3-ft by 5-ft tunnel. These results will be re-plotted and compared in more detail in the following. At the end of the Navier-Stokes simulation, wall pressure distributions are computed and saved. Utilizing the wall pressure distributions as the boundary condition, interference flow field can be obtained to derive the upwash and blockage corrections.

Case 1 (reference, k=0.167, $\alpha_{mean}$=20 °, $\alpha_{amp}$ = 5 °) is one of the three cases presented in Figs. 11-15. The results in free air and tunnel are directly compared. As indicated earlier, the model in tunnel shows higher values at the same angles of attack for lift and drag coefficients. For the pitching moment, greater negative values are obtained for the model in tunnel. This clearly indicates the necessity of wall interference corrections. The interference flow fields computed by solving the Euler equations with the wall pressure distributions are the forcing function. The amount of corrections for the vortex strength of Fig. 11 is similar to that for the lift coefficient in terms of $\alpha$. Vortex position, however, doesn't reflect the wall interference effects in current research. To find average correction factors for the total forces and moment, weighted averages over the whole wing surface area are computed and indicated in Fig. 12 for both upwash and dynamic pressure ratio. Upwash correction is around 1.21 degrees and dynamic pressure increased by 2.25 % at $\alpha$ = 20 in the tunnel. Both upwash and blockage corrections show some hysteresis.

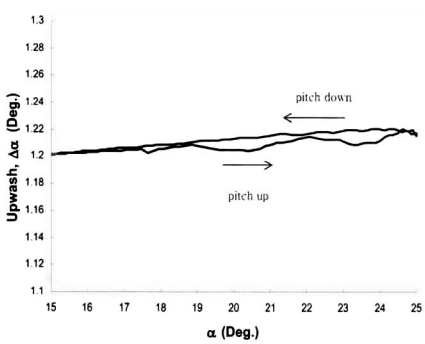


Fig. 12. Upwash by the Wall (Case 1)

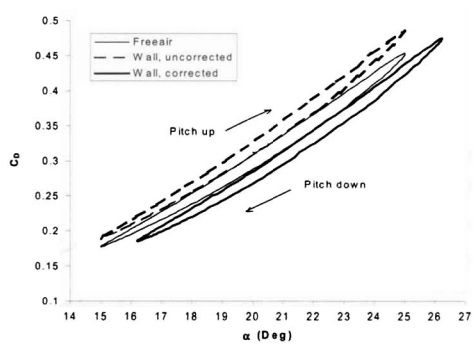


Fig. 13. Corrected Results (Case 1)

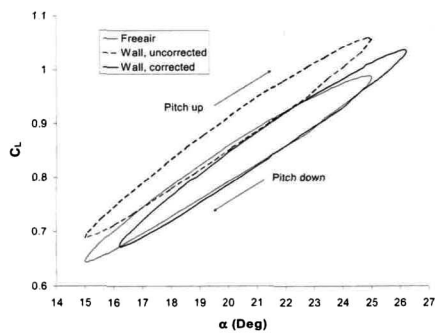


**Fig. 14. Corrected Results (Case 1)**

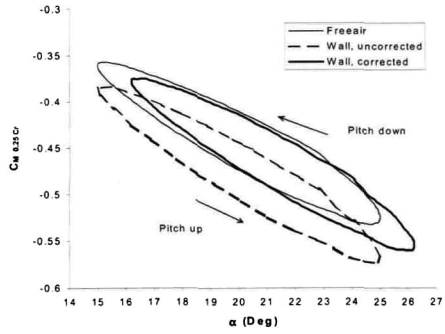


**Fig. 15. Corrected Results (Case 1)**

In Fig. 16, aerodynamic coefficients for Case 2 (small reduced frequency, k=0.067, $\alpha_{mean}$=20 °, $\alpha_{amp}$ = 5 °) are compared. As in the Case 1, the model in tunnel develops higher lift and drag coefficients. However, the amount of hysteresis is less than that of Case 1 because the reduced frequency is much lower. Upwash correction is about 1.07 degrees and dynamic pressure increased by 1.7 % at $\alpha_{mean}$=20 ° in the tunnel. The correction factors for Case 2 results in the smaller hysteresis than for Case 1, in particular in the blockage correction. Therefore, at low reduced frequencies, static correction factors should be sufficient for dynamic testing.

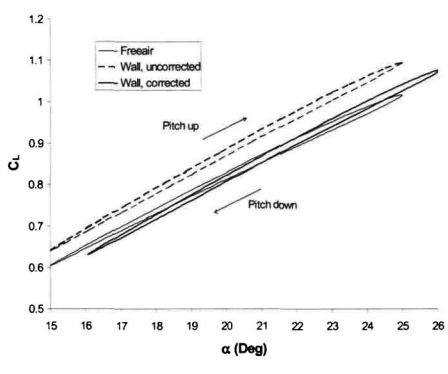


**Fig. 16. Corrected Results (Case 2)**

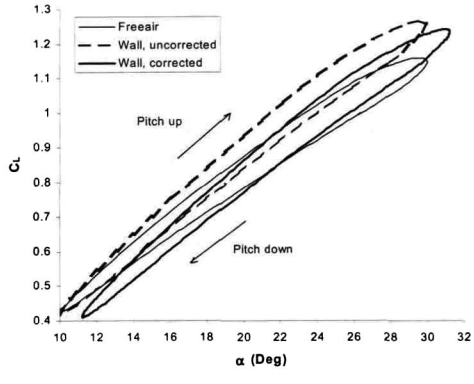


**Fig. 17. Corrected Results (Case 3)**

The computed results of Case 3 (large amplitude, k=0.167, $\alpha_{mean}$=20° , $\alpha_{amp}$ = 10 °) in tunnel and free air are compared in Fig. 17. As in the Cases 1 and 2, the model in tunnel shows higher values and significant increase in slopes with the angle of attack than in free air for the lift and drag coefficients. But, the amount of hysteresis is greater than that of Cases 1 and 2. It is also seen that the interference effect is small at low angles of attack such as $\alpha$=10. The hysteresis characteristics are now more obvious than the previous two cases (Figures 13 and 16). Typically, the wall pressure distributions exhibit larger differences between the floor and ceiling values than Cases 1 and 2. Upwash correction is about 1.4 degrees and the blockage correction is 1.027 at $\alpha_{mean}$=20 in the tunnel.

Finally, the upwash and blockage corrections are applied to the computed results of the models in the wind tunnel, as described in Chapter 4. In Figs. 13-15 of Case 1, lift and moment coefficients show very good agreement with the results in free air. However, the drag coefficient is over-corrected. One possible reason is that the present drag calculation under dynamic conditions may not be accurate because of inaccurate turbulence model. The same comments are applicable to the corrected results for Case 2 (Fig. 16). For Case 3 as shown in Fig. 17 the corrections at low angles of attack are somewhat excessive.

## Conclusions

A numerical method for the assessment and correction of tunnel wall interference effects in forced-oscillation testing was presented. The wall pressure field was computed using an unsteady three dimensional full Navier-Stokes solver for a 70-degree pitching delta wing in a wind tunnel. The computed wall pressure field was then imposed as boundary conditions for Euler re-simulation to obtain the interference flow field.

The calculated static results were shown in good agreements with some experimental data. The flow field around pitching delta wings was investigated for k=0.376, $\alpha_{mean}$=27 ° and $\alpha_{amp}$ = 27 °. Tunnel interference effect on the vortex strength showed a similar trend in upwash effects as on aerodynamic coefficients. Parametric analysis of blockage and upwash effects for models with different amplitudes and reduced frequencies were made. For the larger amplitude and reduced frequency, flow hysteresis and wall interference effects were greater. The results of the model in tunnel were corrected by the wall pressure signature method. The corrected results showed good agreements with the computed results in free air, except at low $\alpha$ with a large amplitude and high frequency employed in the computation.

## References

1. Wentz, William H., "Wind tunnel Investigations of Vortex Breakdown on Slender Sharp-Edged Wings," Ph.D. Dissertation, The University of Kansas.

2. Wolffelt,K.W., "Investigation of the Movement of Vortex Burst Position with Dynamically Changing Angle of Attack for a Schematic Delta Wing in a Water Tunnel with Correlation to Similar Studies in a Wind Tunnel," AGARD-CP-413, 1986.

3. Soltani M.R., Bragg, M.B. and Brandon, J.M., "Experimental Measurements on an Oscillating 70-Degree Delta Wing in Subsonic Flow," AIAA Paper 88-2576, 1988.

4. Torlund, P., "Wind Tunnel Force Measurements and Visualization on a 60-Degree Delta Wing in Oscillation, Stepwise Motion and Gusts," AGARD-CP-497, 1991.

5. Fujii, K. and Schiff, L.B., "Numerical Simulation of Vortical Flows over a Strake-Delta Wing," *AIAA Journal*, Vol. 27, No. 9, 1989, pp.1153-1162.

6. Hartwich, P.M., and Hsu, C.M., "Numerical Study of the Vortex Burst Phenomenon for Delta Wings," AIAA Paper 88-0505, 1988.

7. Ekaterinaris, J. A., Coutley, R.L., Schiff, L.B. and Platzer, M.F., Numerical Investigation of the Flow over a Delta Wing at High Incidence," AIAA Paper 91-0753, 1991.

8. Kandil, O.A. and Chuang, H. A., "Unsteady Navier-Stokes Computations past Oscillating Delta Wing at High Incidence," AIAA Paper 89-0081, 1989.

9. Chaderjian, N.M. and Guruswamy, G. P., "Transonic Navier-Stokes Computations for an Oscillating Wing Using Zonal Grids," *Journal of Aircraft*, Vol. 29, No. 3, 1992, pp. 326-335.

10. Ewald, B.F.R., Editor, "Wind Tunnel Wall Correction" AGARDograph 336, 1998.

11. Thomas, J.P. and Lan, C.E., "The Simulation and Correction of Wind Tunnel Wall Interference on Delta Wing Lift Using Navier-Stokes and Euler Solutions," AIAA Paper 91-3300, 1991

12. Hsing, C.A. and Lan, C.E., "Low Speed Wind Tunnel Interference Assessment/Correction with Vortex Flow Effect," *Journal of Aircraft*, Vol. 34, No. 2, 1997, pp. 220-227.

13. Pulliam, T. H., "Euler and Thin Layer Navier Stokes Codes: ARC2D, ARC3D," Notes for the Computational Fluid Dynamics User's Workshop, University of Tennessee Space Institute, Tullahoma, Tennessee, Mar. 12-16, 1984.

14. Hoffmann, K. A., *Computational Fluid Dynamics for Engineers*, Engineering Education System, Austin, 1989.

15. Soltani M.R., Bragg, M.B. and Brandon, J.M., "Measurements on an Oscillating 70-Deg Delta Wing in Subsonic Flow," *Journal of Aircraft*, Vol. 27, No. 3, March 1990.

16. Brandon, J.M. and Shah, G.H., "Effect of Large Amplitude Pitching Motions on the Unsteady Aerodynamic Characteristics of Flat-Plate Wings," AIAA Paper 88-4331, 1988.